Journal of Materials Science: Materials in Electronics (2018) 29:18859–18867
https://doi.org/10.1007/s10854-018-0011-3

Enhanced energy storage properties in MgO-doped $BaTiO_3$ lead-free ferroelectric ceramics

Gang Liu[1] · Leiyang Zhang[1] · Qiankun Wu[1] · Ziyang Wang[2] · Yang Li[1] · Dequan Li[1] · Hongbo Liu[3] · Yan Yan[1]

Received: 25 February 2018 / Accepted: 5 September 2018 / Published online: 8 September 2018

Abstract
In this investigation, MgO-doped $BaTiO_3$ (BT) ceramics were prepared by a conventional solid-state sintering method. Perovskite-structure was identified by an X-ray diffraction method. Relatively high volume density and relative density were achieved with appropriate MgO contents. With MgO doping, the temperature stability of the dielectric constant of BT samples was drastically improved when the temperature is below their Curie temperatures. It is very interesting that both the energy storage density and breakdown electric field are enhanced by MgO doping compared to that of undoped BT. Particularly, a high energy storage density (W_c) of 0.9 J/cm^3 can be achieved at 130 kV/cm with a high energy storage efficiency (η) of 73.3% in 0.25 wt% MgO doped composition. The detailed investigation and analysis can be found in the study.

1 Introduction

In the past decades, dielectric ceramic materials have attracted much attention because of their large dielectric constant and rapid charge and discharge rates, which makes them suitable for the potential applications in pulse power capacitors as the capacitive components [1–15]. Among the dielectric ceramics, ferroelectric ceramics have been extensively investigated for the potential pulse power capacitors. Generally speaking, an excellent candidate of ferroelectric ceramics for the aforementioned application must possess large saturated polarization (P_s), small remnant polarization (P_r) and high breakdown electric field strength (E_b) simultaneously, based on the characteristics of polarization–electric field (P–E) hysteresis loops [16]. On one hand, since $Pb(Mg_{1/3}Nb_{2/3})O_3$ as the relaxor ferroelectric system was first reported [17], a lot of excellent performances have been discovered in Pb-based relaxor ferroelectrics. On the other hand, according to the theory the relaxor ferroelectrics can fulfil the aforementioned requirements such as large P_s, small P_r and high E_b, they have hence been widely investigated potentially as the pulse power capacitors. Unfortunately, due to the environment and human health concerns, lead-free relaxor ferroelectrics have attracted a lot attention in the past decade [13, 18–23]. Most recently, perovskite structural lead-free $(1-x)$BT–xBi(Me)O_3 (Me = Mg, Nb, Sc, Zn, Ti, etc.) solid solutions have become a research topic since their very excellent relaxor nature, especially the excellent performance in energy storage [6, 9, 13, 24–26]. For instance, energy storage densities of 1.13 J/cm^3 and 1.81 J/cm^3 were reported in $0.9BaTiO_3$–$0.1Bi(Mg_{2/3}Nb_{1/3})O_3$ [9] and $0.88BaTiO_3$–$0.12Bi(Mg_{1/2}Ti_{1/2})O_3$ [8] systems, respectively. It is known that the $(1-x)$BT–xBi(Me)O_3 systems are not easy to synthesis because of the difference in sintering temperatures between BT and Bi(Me)O_3. Hence, a simple relaxor system with better densification condition would be very attractive in the energy storage applications, which will benefit the manufacture.

Until now, the effects of MgO dopant on the microstructures and dielectric properties have been investigated and reported by several research groups [27–30]. Unfortunately, the energy storage properties in this system are still lacking. Hence, we try to introduce MgO into BT ceramics in the current paper, and the energy storage properties were investigated. The detailed results are demonstrated and discussed in the current paper.

✉ Gang Liu
liugangswu@126.com

✉ Yan Yan
yanyan2013@swu.edu.cn

[1] Faculty of Materials and Energy, Southwest University, Chongqing 400715, China

[2] Hanhong College, Southwest University, Chongqing 400715, China

[3] School of Materials Engineering, Shanghai University of Engineering Science, Shanghai 201620, China

2 Experimental procedure

Conventional electroceramic preparation route was employed to fabricate $BaTiO_3$–x wt% MgO ($x = 0$, 0.25, 0.5, 0.75, 1 and 3) ceramics using $BaTiO_3$ (Sinocera Barium Titanate, 99%, Shandong) and MgO (Aladdin, 99.99%, Shanghai) powders as the raw materials. The powders with appropriate ratio were ball-milled in alcohol for 24 h. Powders after drying with 5 wt% PVA were die-pressed to obtain the small green compacts with a diameter of 10 mm. The green samples were debinded at 500 °C in air, and fired at various sintering temperatures from 1300 to 1460 °C for 2 h. The densities of the sintered ceramic samples were measured by the Archimedes' method. X-ray diffractometer (6100, Shimadzu, Japan) with monochromatic Cu Kα radiation was utilized to check the phases with 2θ ranging from 20° to 70°. Scanning electron microscope (JSM 6610, Jeol, Tokyo, Japan) was employed to observe the fractured surface of the ceramic samples. Electrodes were made on each side of the sintered ceramics for electrical properties measurement. The temperature-dependent dielectric properties were measured at various frequencies from room temperature to 175 °C using a LCR meter (E4980AL, Keysight, USA). The polarization–electric field (P–E) hysteresis loops under different temperatures were carried out with a Sawyer–Tower circuit (TF analyzer 2000E, aixACCT, Aachen, Germany) under 10 Hz within an environmental chamber.

3 Results and discussion

The XRD patterns at room temperature of the MgO-doped and undoped BT ceramic samples are exhibited in Fig. 1. When the 2θ ranging from 20° to 70°, all the samples show a single perovskite-structure without any second phase. As displayed in Fig. 1, all the diffraction peaks are all indexed clearly. So it can be observed that for undoped BT, a tetragonal phase is identified as suggested by the strong peak splitting at the 2θ around 45°. In contrast, for the MgO-doped BT samples, the peak splitting at the 2θ around 45° cannot be detected, so a cubic symmetry is suggested by the XRD patterns, also implying that the lattice distortion has been decreased drastically. Jeong and Han doped Mg ion in BT to replace Ti ion, and they obtained $Ba(Ti_{1-x}Mg_x)O_{3-x}$ ceramics [28]. In their work, it has been found that introducing Mg into the BT would still keep the tetragonal symmetry for BT. Especially, when the addition of Mg ion exceeds 2%, a second hexagonal phase was formed. Unfortunately, in our case, it seems that with extra MgO in stoichiometry BT, the transition of the structures is different from that of Jeong and Han' work.

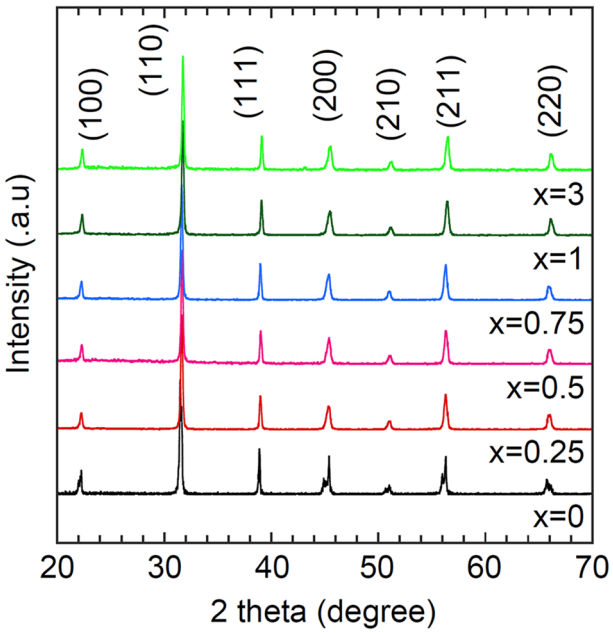

Fig. 1 Room temperature X-ray diffraction patterns for ceramics with different MgO contents from 20° to 70°

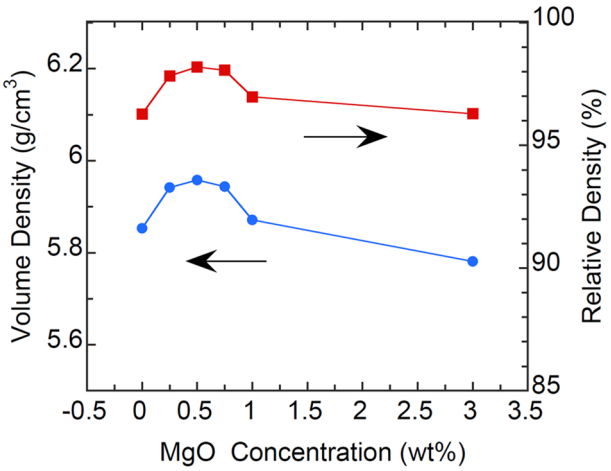

Fig. 2 Volume density and relative density as a function of MgO doping content

The volume density and relative density as a function of MgO content are exhibited in Fig. 2. It is clear that both the volume density and relative density are increased effectively with MgO addition, and the highest value is achieved at the composition with 0.5 wt% MgO. Further increase of MgO leads to a decrease of density. Figure 3 shows the SEM photos and it reveals that the undoped BT has polygonal grains with an average grain size around 10 μm. In contrast, in the 0.25 and 0.5 wt% MgO doped samples, irregular grain

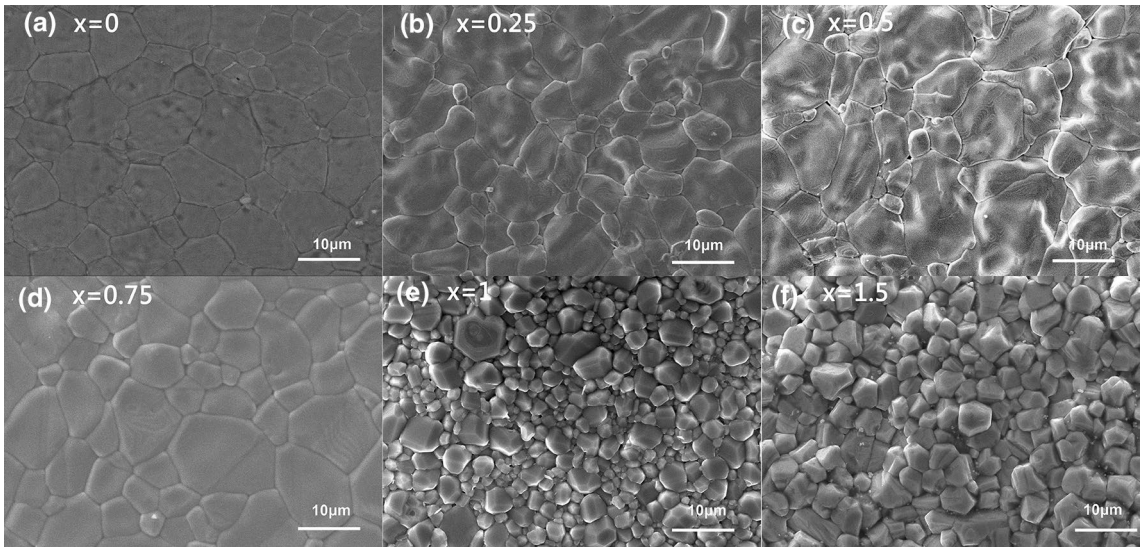

Fig. 3 SEM images of MgO-doped and undoped BT ceramics. **a** x = 0, **b** x = 0.25, **c** x = 0.5, **d** x = 0.75, **e** x = 1 and **f** x = 3

boundaries are observed, as shown in Fig. 3b, c, indicating that liquid phase appears during sintering in these compositions. It is known that with the assistance of liquid phase during densification, high volume density and relative density can be achieved. However, with further increasing the MgO content, the grain growth is inhibited and densification becomes difficult, resulting in a relatively loose structure. This might be the reason for the decrease of volume density and relative density of the compositions with higher MgO concentrations.

Figure 4 shows the dielectric properties of the sintered ceramics as a function of temperature determined at various frequencies from room temperature to 200 °C. A typical dielectric peak at the temperature of 130 °C can be observed in Fig. 4a, which suggests a first order ferroelectric to paraelectric phase transition, and is also in good agreement with previous report [31]. The corresponding dielectric loss also exhibits an anomaly at a similar temperature. Moreover, once the MgO is introduced into the BT system, the dielectric constant at the peak decreases rapidly from 10,000 to 2300. Because the ionic radius of Mg^{2+} (0.72 Å) is very close to that of Ti^{4+} (0.64 Å), it is highly likely that Mg^{2+} ions will substitute for Ti^{4+} to generate B-site acceptor doping behavior. The presence of Mg acceptor defects in $BaTiO_3$ ceramics leads to the formation of cubic structures, as indicated in the Fig. 1. The cubic symmetry implies that the lattice distortion has been decreased. It finally leads to the decrease of the dielectric constant. However, this change of dielectric constant is beneficial to the improvement of temperature stability, which is very consistent with previous reports. Regardless of doping concentration, the T_C of these MgO-doped BT samples is always around 128–130 °C. When the temperature decreases from T_C to room temperature, the decrease of dielectric constant is not as obvious as that in pure BT samples. A relatively low dielectric constant around 1800 is observed in 0.25, 0.5 and 0.75 wt% MgO doped compositions. Moreover, with further increase of MgO, the dielectric constant is increased to around 2200 and 2000 for 1 and 3 wt% MgO doped samples, respectively. Therefore, based on the comparison with pure BT, MgO doping has shown obvious effect on peak broadening and depressing, which is consistent with the aforementioned analysis. Especially, MgO doping is effective to flat the dielectric constant below their T_C compared with pure BT. This feature is completely different from the features observed in relaxor ferroelectrics, where broad dielectric peaks with strong dielectric dispersions are observed at the same time [20, 32–34].

Beside the variations of the dielectric properties, the *P–E* hysteresis loops of the prepared samples also show obvious variations with respect to the MgO content. As shown in Fig. 5a, typically square *P–E* hysteresis loops are observed in undoped BT. A P_{max} of 31.5 μC/cm^2 and a E_c (coercive field) around 5 kV/cm are observed at the maximum electric field of 100 kV/cm. However, the large hysteresis in the *P–E* loops makes BT not suitable for energy storage application, since a large hysteresis would lead to a large energy loss [16]. It is very interesting that with introducing MgO into BT, the corresponding *P–E* loops become slants. Both the P_r and E_c are decreased as the MgO content increased, accompanying with a large decrease of the hysteresis in *P–E* loops. The shapes of these hysteresis loops for MgO-doped BT are very similar to those for relaxor ferroelectrics, although their dielectric

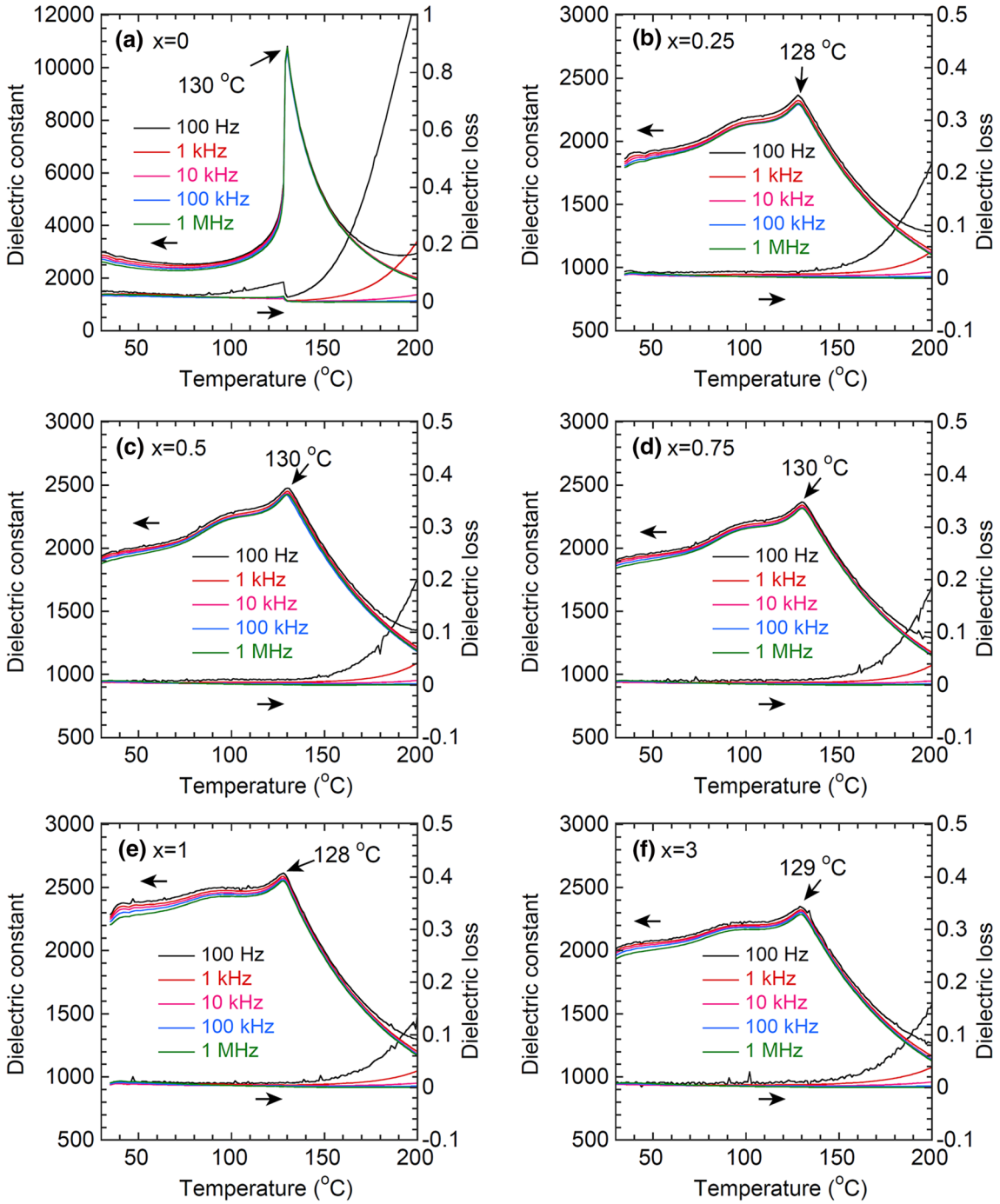

Fig. 4 Dielectric constant and dielectric loss as a function of temperature measured at various frequencies from room temperature to 200 °C. **a** x = 0, **b** x = 0.25, **c** x = 0.5, **d** x = 0.75, **e** x = 1 and **f** x = 3

properties show obvious differences [20, 32, 35, 36]. In 0.25 wt% MgO doped composition, the E_b is increased to 130 kV/cm, which is nearly 30% increase compared to that of undoped BT. The reason is very clear the cubic structures formed by MgO doping belong to the paraelectric phases rather than ferroelectric phases, which will directly decrease the ferroelectric properties of the $BaTiO_3$ samples.

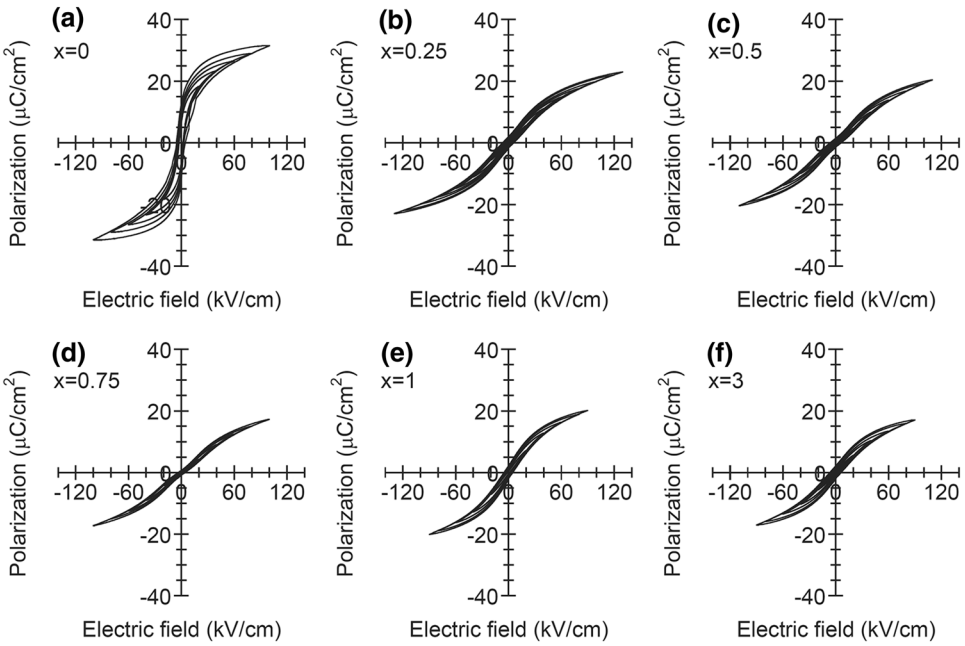

Fig. 5 Room temperature polarization–electric field (*P–E*) hysteresis loops measured at different electric field strengths. **a** x = 0, **b** x = 0.25, **c** x = 0.5, **d** x = 0.75, **e** x = 1 and **f** x = 3

With the *P–E* hysteresis loops, the energy storage density (W_c) and energy storage efficiency η can be calculated by the following equations [37]:

$$W_c = \int_0^{P\max} Edp, \tag{1}$$

$$W_d = -\int_{P\max}^{P_r} Edp, \tag{2}$$

$$\eta = \frac{W_d}{W_c} \times 100\%, \tag{3}$$

where $P_{\max}$ and P_r stand for the maximum polarization and remnant polarization, respectively. Figure 6a shows the W_c of MgO-doped BT ceramics as a function of the electric field. For undoped BT, a maximum W_c around 0.39 J/cm^3 is obtained at an electric field of 100 kV/cm. In contrast, even at the same electric field, MgO-doped BT ceramics show superior W_c (0.66 J/cm^3) over that of undoped BT. It is very interesting that the 0.25 wt% MgO doped ceramic shows a high W_c of 0.9 J/cm^3 at an electric field of 130 kV/cm. The η as a function of electric field for MgO-doped BT ceramics is also shown in Fig. 6b. For the undoped BT, the η is around 38–53% when the electric field is increased from 10 to 100 kV/cm. While, the η of the MgO-doped ceramics is enhanced effectively. At small electric field (10 kV/cm), a high η (above 85%) is observed in all doped compositions. Even the field is increased to 130 kV/cm, the η of 0.25 wt% MgO-doped composition is still around 73.4%, indicating a high energy storage efficiency. Figure 6c exhibits the W_c and η values at different electric fields. At an electric field of 20 kV/cm, the W_c seems independent with the electric field. However, at higher electric field, such as 80 kV/cm, the maximum W_c (0.5 J/cm^3) can be observed in both 0.25 and 0.5 wt% MgO doped compositions. Meanwhile, the maximum η (80%) is also obtained at the same compositions, implying that these compositions possess the superior energy storage properties over other compositions. Although the dielectric and ferroelectric properties are not enhanced for MgO-doped samples, the energy storage properties are effectively improved. It can be explained by the following part. According to Eq. (1), large dielectric constant ($P_{\max}$) and small E_b are not enough to obtain a high energy storage density. Oppositely, proper dielectric constant and strength of electric fields can lead to better energy storage density. When MgO was doped into $BaTiO_3$, the dielectric constant was decreased, but it can match well with the increased strength of electric fields, finally leading to the improved energy storage density. Moreover, the doping of MgO results in the decrease of dielectric loss, which contributes much to the improvement of energy storage efficiency.

Figure 7 shows the *P–E* hysteresis loops as a function of temperature of the obtained BT ceramics. For the undoped BT, its *P–E* loops become slim at first, and then broaden

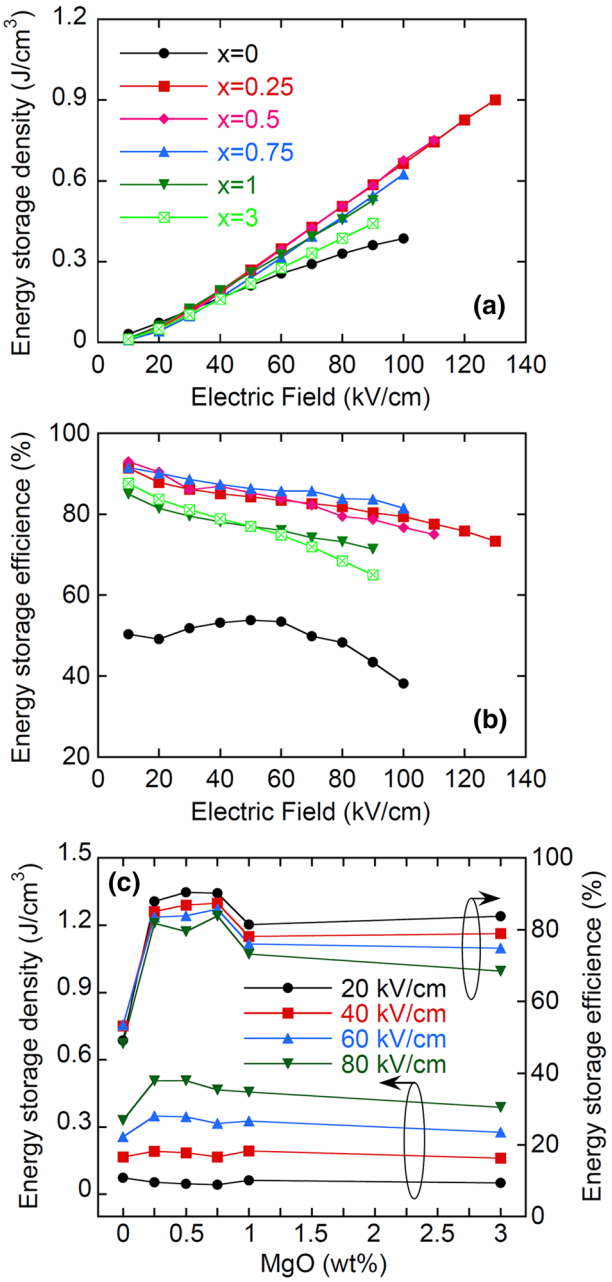

Fig. 6 Room temperature **a** energy storage density (J_d) and **b** energy storage efficiency (η) for MgO-doped BT ceramics. **c** J_d and η as a function of MgO contents measured at 20, 40, 60 and 80 kV/cm

when the temperature is more than 125 °C. According to the literature, it is likely that when the temperature increases, the long-range order in ferroelectric phase would be disturbed, and thus results in a decrease of polarization [16]. That is why *P–E* loops become slim as temperature increases. When the temperature is beyond T_C, the *P–E* loops normally become slimmer according to previous reports. However, as shown in Fig. 7a, the broadening of the *P–E* loops must be correlated to a conductive contribution [38, 39], which increase the dielectric loss at high temperature. Moreover, it is very interesting that although the P_{max} and P_r are decreased greatly, the temperature stability of the *P–E* loops in all MgO-doped compositions is effectively enhanced. Even the temperature is increased up to 200 °C, the P_{max} shows a little variation with respect to the temperature. Of course, the increase of P_r at high temperature region (about 125 °C) is due to the same mechanism as indicated in undoped BT ceramic.

Figure 8 shows the W_c and η as a function of temperature from 25 to 200 °C measured at various electric fields for undoped and doped BT ceramics. In general, for commercial electronic devices, the working temperature is normally below 125 °C. The W_c and η of the undoped BT samples vary from 0.15–0.22 J/cm^3 and 45.6–60.7%, respectively, when the temperature increases from 25 to 125 °C with an electric field of 50 kV/cm. In contrast, in all MgO doped compositions, the variation of W_c and η is smaller than that of undoped BT. For example, the W_c and η of 0.25 wt% MgO-doped BT from 25 to 125 °C are 0.23–0.26 J/cm^3 and 85.6–87.5%, respectively. These characteristics suggest that MgO doped BT ceramics can be considered as potential materials for energy storage capacitors.

4 Conclusions

In summary, the lead-free *x*MgO-doepd $BaTiO_3$ (BT) with $x = 0$, 0.25%, 0.5%, 0.75%, 1% and 3% ceramics were prepared by a conventional electroceramic fabrication process. Single phase perovskite-structure for all studied compositions was identified by an X-ray diffraction method. With introducing the MgO into BT, the temperature stability of the dielectric constant was improved drastically when the temperature is below their Curie temperatures; while the Curie temperatures of these compositions are independent to the MgO doping. A high W_c of 0.9 J/cm^3 and η of 73.3% can be achieved at an electric field of 130 kV/cm within 0.25 wt% MgO doped BT samples. The temperature dependent W_c and η at different electric fields were also evaluated. Highly stable W_c and η below the Curie temperature demonstrate that the MgO-doped BT ceramics can be a very useful material for dielectric capacitors for potential applications.

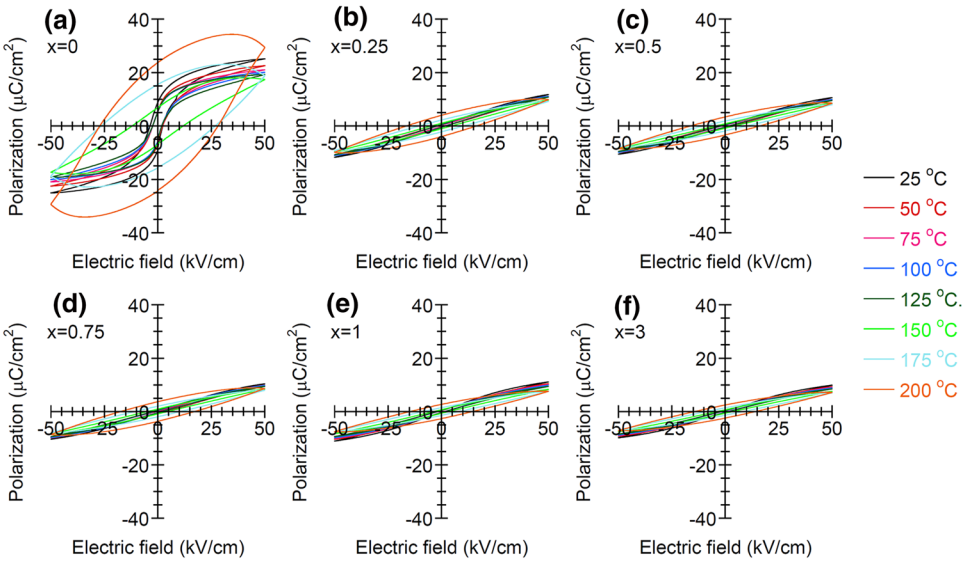

Fig. 7 *P–E* hysteresis loops measured from 25 to 200 °C with an interval of 25 °C. **a** x = 0, **b** x = 0.25, **c** x = 0.5, **d** x = 0.75, **e** x = 1 and **f** x = 3

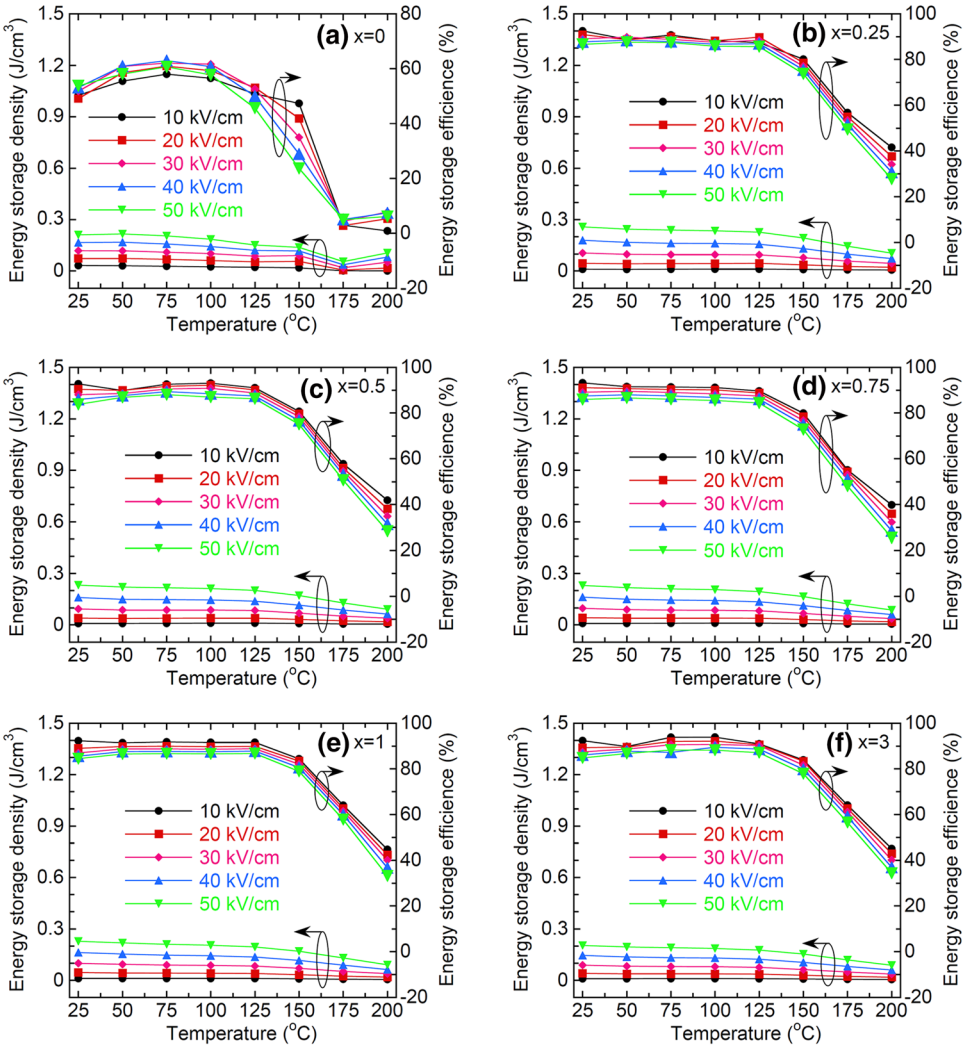

Fig. 8 J_d and η as a function of temperature from 25 to 200 °C measured at 10, 20, 30, 40, and 50 kV/cm. **a** x = 0, **b** x = 0.25, **c** x = 0.5, **d** x = 0.75, **e** x = 1 and **f** x = 3

Acknowledgements The work is supported by the National Natural Science Foundation of China (51672226, 51502248, 11704242); Natural Science Foundation of Shanghai, China (17ZR1447200); Fundamental Research Funds for the Central Universities (XDJK2017D013, XDJK2017D021); National College Student innovation and Entrepreneurship Program of Southwest University (201710635057, 201710635015).

References

1. I. Burn, D.M. Smyth, Energy storage in ceramic dielectrics. J. Mater. Sci. **7**(3), 339 (1972)
2. N.H. Fletcher, A.D. Hilton, B.W. Ricketts, Optimization of energy storage density in ceramic capacitors. J. Phys. D **29**(1), 253 (1996)
3. V.S. Puli, D.K. Pradhan, D.B. Chrisey, M. Tomozawa, G.L. Sharma, J.F. Scott, R.S. Katiyar, Structure, dielectric, ferroelectric, and energy density properties of (1−x)BZT−xBCT ceramic capacitors for energy storage applications. J. Mater. Sci. **48**(5), 2151–2157 (2013)
4. T. Wang, X. Wei, Q. Hu, L. Jin, Z. Xu, Y. Feng, Effects of $ZnNb_2O_6$ addition on $BaTiO_3$ ceramics for energy storage. Mater. Sci. Eng. B **178**(16), 1081–1086 (2013)
5. X. Wei, H. Yan, T. Wang, Q. Hu, G. Viola, S. Grasso, Q. Jiang, L. Jin, Z. Xu, M.J. Reece, Reverse boundary layer capacitor model in glass/ceramic composites for energy storage applications. J. Appl. Phys. **113**(2), 024103 (2013)
6. Z. Song, H. Liu, S. Zhang, Z. Wang, Y. Shi, H. Hao, M. Cao, Z. Yao, Z. Yu, Effect of grain size on the energy storage properties of $(Ba_{0.4}Sr_{0.6})TiO_3$ paraelectric ceramics. J. Eur. Ceram. Soc. **34**(5), 1209–1217 (2014)
7. T. Wang, L. Jin, Y. Tian, L. Shu, Q. Hu, X. Wei, Microstructure and ferroelectric properties of Nb_2O_5-modified $BiFeO_3$-$BaTiO_3$ lead-free ceramics for energy storage. Mater. Lett. **137**, 79–81 (2014)
8. Q. Hu, L. Jin, T. Wang, C. Li, Z. Xing, X. Wei, Dielectric and temperature stable energy storage properties of $0.88BaTiO_3$-$0.12Bi(Mg_{1/2}Ti_{1/2})O_3$ bulk ceramics. J. Alloys Compd. **640**, 416–420 (2015)
9. T. Wang, L. Jin, C. Li, Q. Hu, X. Wei, Relaxor ferroelectric $BaTiO_3$-$Bi(Mg_{2/3}Nb_{1/3})O_3$ ceramics for energy storage application. J. Am. Ceram. Soc. **98**(2), 559–566 (2015)
10. R.A. Malik, A. Hussain, A. Maqbool, A. Zaman, T.K. Song, W.J. Kim, M.-H. Kim, Giant strain, thermally-stable high energy storage properties and structural evolution of Bi-based lead-free piezoceramics. J. Alloys Compd. **682**, 302–310 (2016)
11. Y. Tian, L. Jin, H. Zhang, Z. Xu, X. Wei, E.D. Politova, S.Y. Stefanovich, N.V. Tarakina, I. Abrahams, H. Yan, High energy density in silver niobate ceramics. J. Mater. Chem. A **4**(44), 17279–17287 (2016)
12. Z. Yang, H. Du, S. Qu, Y. Hou, H. Ma, J. Wang, J. Wang, X. Wei, Z. Xu, Significantly enhanced recoverable energy storage density in potassium-sodium niobate-based lead free ceramics. J. Mater. Chem. A **4**(36), 13778–13785 (2016)
13. Q. Hu, T. Wang, L. Zhao, L. Jin, Z. Xu, X. Wei, Dielectric and energy storage properties of $BaTiO_3$–$Bi(Mg_{1/2}Ti_{1/2})O_3$ ceramic: influence of glass addition and biasing electric field. Ceram. Int. **43**(1), 35–39 (2017)
14. T. Shao, H. Du, H. Ma, S. Qu, J. Wang, J. Wang, X. Wei, Z. Xu, Potassium-sodium niobate based lead-free ceramics: novel electrical energy storage materials. J. Mater. Chem. A **5**(2), 554–563 (2017)
15. Y. Tian, L. Jin, H. Zhang, Z. Xu, X. Wei, G. Viola, I. Abrahams, H. Yan, Phase transitions in bismuth-modified silver niobate ceramics for high power energy storage. J. Mater. Chem. A **5**(33), 17525–17531 (2017)
16. L. Jin, F. Li, S. Zhang, Decoding the fingerprint of ferroelectric loops: comprehension of the material properties and structures. J. Am. Ceram. Soc. **97**(1), 1–27 (2014)
17. F. Li, L. Wang, L. Jin, D. Lin, J. Li, Z. Li, Z. Xu, S. Zhang, Piezoelectric activity in Perovskite ferroelectric crystals. IEEE Trans. Ultrason. Ferroelectr. Freq. Control **62**(1), 18–32 (2015)
18. T.R. Shrout, S.J. Zhang, Lead-free piezoelectric ceramics: alternatives for PZT? J. Electroceram. **19**(1), 113–126 (2007)
19. D. Damjanovic, N. Klein, J. Li, V. Porokhonskyy, What can be expected from lead-free piezoelectric materials? Funct. Mater. Lett. **3**(1), 5–13 (2010)
20. V.V. Shvartsman, D.C. Lupascu, Lead-free relaxor ferroelectrics. J. Am. Ceram. Soc. **95**(1), 1–26 (2012)
21. F. Li, L. Jin, R. Guo, High electrostrictive coefficient Q33 in lead-free $Ba(Zr_{0.2}Ti_{0.8})O_3$-$x(Ba_{0.7}Ca_{0.3})TiO_3$ piezoelectric ceramics. Appl. Phys. Lett. **105**(23), 232903 (2014)
22. L. Jin, R. Huo, R. Guo, F. Li, D. Wang, Y. Tian, Q. Hu, X. Wei, Z. He, Y. Yan, G. Liu, Diffuse phase transitions and giant electrostrictive coefficients in lead-free Fe^{3+}-doped $0.5Ba(Zr_{0.2}Ti_{0.8})O_3$-$0.5(Ba_{0.7}Ca_{0.3})TiO_3$ ferroelectric ceramics. ACS Appl. Mater. Interfaces **8**(45), 31109–31119 (2016)
23. Q. Hu, L. Jin, P.S. Zelenovskiy, V.Y. Shur, Y. Zhuang, Z. Xu, X. Wei, Relaxation behavior and electrical inhomogeneity in $0.9BaTiO_3$-$0.1Bi(Mg_{1/2}Ti_{1/2})O_3$ ceramic. Ceram. Int. **43**(15), 12828–12834 (2017)
24. H. Ogihara, C.A. Randall, S. Trolier-McKinstry, High-Energy Density Capacitors Utilizing 0.7 $BaTiO_3$–0.3 $BiScO_3$ Ceramics. J. Am. Ceram. Soc. **92**(8), 1719–1724 (2009)
25. H. Ogihara, C.A. Randall, S. Trolier-McKinstry, Weakly coupled relaxor behavior of $BaTiO_3$–$BiScO_3$ ceramics. J. Am. Ceram. Soc. **92**(1), 110–118 (2009)
26. D.H. Choi, A. Baker, M. Lanagan, S. Trolier-McKinstry, C. Randall, Structural and dielectric properties in $(1-x)BaTiO_3$–$xBi(Mg_{1/2}Ti_{1/2})O_3$ ceramics ($0.1 \le x \le 0.5$) and potential for high-voltage multilayer capacitors. J. Am. Ceram. Soc. **96**(7), 2197–2202 (2013)
27. J. Jeong, Y.H. Han, Electrical properties of MgO-doped $BaTiO_3$. Phys. Chem. Chem. Phys. **5**(11), 2264–2267 (2003)
28. J.S. Park, Y.H. Han, Effects of MgO coating on microstructure and dielectric properties of $BaTiO_3$. J. Eur. Ceram. Soc. **27**(2), 1077–1082 (2007)
29. J.S. Park, M.H. Yang, Y.H. Han, Effects of MgO coating on the sintering behavior and dielectric properties of $BaTiO_3$. Mater. Chem. Phys. **104**(2), 261–266 (2007)
30. Y.H. Huang, Y.J. Wu, W.J. Qiu, J. Li, X.M. Chen, Enhanced energy storage density of $Ba_{0.4}Sr_{0.6}TiO_3$–MgO composite prepared by spark plasma sintering. J. Eur. Ceram. Soc. **35**(5), 1469–1476 (2015)
31. B. Jaffe, W.R.J. Cook, H. Jaffe, *Piezoelectric Ceramics* (Acadmic Press, New York, 1971)
32. L.E. Cross, Relaxor ferroelectrics. Ferroelectrics **76**(3–4), 241–267 (1987)
33. Z.G. Ye, Relaxor ferroelectric complex perovskites: structure, properties and phase transitions. Key Eng. Mater. **155**(1), 81–122 (1998)
34. Q. Hu, J. Bian, L. Jin, Y. Zhuang, Z. Huang, G. Liu, V.Y. Shur, Z. Xu, X. Wei, Debye-like relaxation behavior and electric field induced dipole re-orientation of the $0.6BaTiO_3$-$0.4Bi(Mg_{1/2}Ti_{1/2})O_3$ ceramic. Ceram. Int. **44**(1), 922–930 (2018)
35. A.A. Bokov, Z.G. Ye, Recent progress in relaxor ferroelectrics with perovskite structure. J. Mater. Sci. **41**(1), 31–52 (2006)
36. F. Li, L. Jin, Z. Xu, S. Zhang, Electrostrictive effect in ferroelectrics: an alternative approach to improve piezoelectricity. Appl. Phys. Rev. **1**(1), 011103 (2014)

37. C. Xu, Z. Liu, X. Chen, S. Yan, F. Cao, X. Dong, G. Wang, High charge-discharge performance of $Pb_{0.98}La_{0.02}(Zr_{0.35}Sn_{0.55}Ti_{0.10})_{0.995}O_3$ antiferroelectric ceramics. J. Appl. Phys. **120**(7), 074107 (2016)
38. M.I. Morozov, D. Damjanovic, Charge migration in $Pb(Zr,Ti)O_3$ ceramics and its relation to ageing, hardening, and softening. J. Appl. Phys. **107**(3), 034106 (2010)
39. T. Wang, J. Hu, H. Yang, L. Jin, X. Wei, C. Li, F. Yan, Y. Lin, Dielectric relaxation and Maxwell-Wagner interface polarization in Nb_2O_5 doped $0.65BiFeO_3$–$0.35BaTiO_3$ ceramics. J. Appl. Phys. **121**(8), 084103 (2017)